THE JOURNAL OF PHYSICAL CHEMISTRY C

ARTICLE

pubs.acs.org/JPCC

Polarized Raman Scattering from a Single, Segmented SnO_2 Wire

Tsachi Livneh,*,† Yigal Lilach,‡ Inna Popov,‡ Andrei Kolmakov,§ and Martin Moskovits∥

†Department of Physics, Nuclear Research Center, Negev, P.O. Box 9001, Beer- Sheva, 84190, Israel

‡The Harvey M. Krueger Family Center for Nanoscience and Nanothechnology, The Hebrew University, Jerusalem 91904, Israel

§Department of Physics, Southern Illinois University, Carbondale, Illinois 62901, United States

∥Department of Chemistry and Biochemistry, University of California, Santa Barbara, California 93106-9510, United States

ABSTRACT: The use of polarized Raman as a means for determining the growth direction in nanowires with rutile structure is described. One finds that polarization angle dependence of various phonon bands can vary greatly even for isomorphic structures such as SnO_2, TiO_2, and RuO_2. As a result, different phonon modes act as the most structure-indicative modes for these three systems, as determined from the polarization angle dependence of their intensities. Polarized Raman measurements were carried out on a single tetragonal (rutile) SnO_2 segmented nanowire with the microscale segments with a prismatic structure growing along [110]. We demonstrate how the calculated effect of the refraction inside the wire, which comes into play when the wire's effective diameter is significantly larger than the wavelength of the exciting light, is essential in explaining the experimental results.

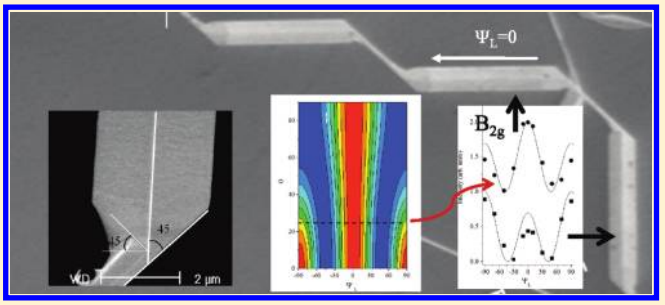

1. INTRODUCTION

Quasi one-dimensional SnO_2 nanostructures have received a great deal of attention recently,[1−9] primarily because of their potential applications in sensors[7] and other electronic and optoelectronic[8] devices but also because of tin oxide's ability to exist in a multitude of nanostructured morphologies such as belts,[1] diskettes,[4] ribbons,[2] and box-beams.[9]

Tin oxide 1D nanowires (indeed quasi 1D nanostructures of most materials) often exist in plural and complex morphologies requiring the determination of the structure and orientation of individual nanowires. This is normally done using electron microscopy/diffraction such as TEM and/or HRTEM and, more recently, synchrotron radiation-based microdiffraction[10] and scanning probe microscopy.[11] These methods require specialized instrumental facilities and sample preparation. However, real world conditions often require in situ determination of a nanowire's structure that has been assembled into a device, especially when its structure evolves during field use. Accordingly, it would be useful to have nanostructure determination using simple and ubiquitous tools that may be used in situ under real world operating conditions.[12−17]

Raman spectroscopy, and specifically polarized Raman, has been used to probe the morphologies of SnO_2,[18] and several other rutile structures including TiO_2,[19] IrO_2,[20] RuO_2,[17,21] and OsO_2.[22] In those studies, the polarization characteristics of single crystals,[18,20,21,22] deposited layers,[19] and nanostructures[17] were used to confirm known structural data obtained by other means. However, the similarity of crystallographic structure is not a sufficient condition for predicting the Raman intensities of the phonons that contribute to the spectrum. For the above materials, both the band frequencies and intensities of the Raman spectra can differ significantly due to the fact that different modes explore different regions of the electron/phonon interactions landscape. In this paper, we compare the expected Raman polarization behavior of three isomorphic materials, which nevertheless possess rather different Raman spectra, SnO_2,[18] TiO_2,[19] and RuO_2,[21] when probed (as is most commonly done) in the backscattered configuration with the light normal to the (100), (110), (101), (001), and (111) rutile planes. This will provide a simple tool box that will facilitate the determination of structural information from polarized Raman of rutile structures.

A complication arises (particularly for micrometer-scale structures) when the incident laser beam is not perpendicular to the apparent surface of the structure but locally strikes the surface at an oblique angle. In such cases, the polarization dependence of the various phonon bands will be affected by the refraction inside the wire especially for large refraction index materials which will impact the Eulerian angles used for transforming between lab-fixed and sample-fixed coordinates and by reflectance losses for both the incident and scattered light.

In a previous publication,[23] we described a method for controlling the structure along the length of single segmented SnO_2 nanowires by controlling the instantaneous material flow rate while the nanostructures were nucleating and growing at constant temperature using vapor−solid (VS) synthesis. Nanowires grown in this way consisted of thick micrometer-scale

Received: March 11, 2011
Revised: June 28, 2011
Published: August 15, 2011

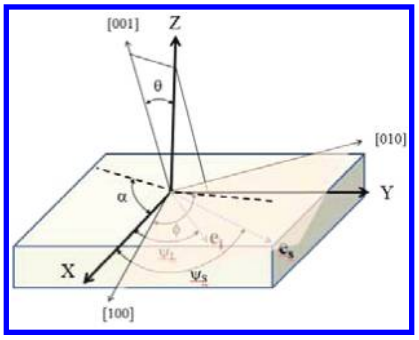

Figure 1. Raman scattering geometry used in this experiment. θ is the angle between the [001] axis in the crystal-fixed coordinates and the Z-axis of the lab-fixed coordinates. ϕ is the angle between the [100] axis and the projection of $\mathbf{k}_s$ on the (001) plane. α is the angle between the X-axis and the projection of the [001] axis onto the $X-Y$ plane of the laboratory coordinates. ψ_L and ψ_S are the angles between the X coordinate and the incoming and scattered polarization vectors, respectively.

segments periodically separated by segments of smaller thickness that grow at ±45° with respect to the former. The nanowires appeared to have a tendency to preserve planarity during their multiple twists and turns, so that (with equal segment lengths) the overall direction of nanowire growth is various combinations of +45° and −45° turns. Furthermore, the thick segments were found to have a prismatic structure, with an angle between the incident laser to the surface estimated to be 45°. This fact must be taken into account when analyzing the polarized Raman signal.

In this paper, we use the aforementioned structurally complex SnO_2 rutile structure as an archetype that illustrates some of the variables that need to be taken into account when using polarized Raman as a complementary technique to HRTEM for determining growth direction.

2. EXPERIMENTAL SECTION

Raman spectra were recorded in a backscattering geometry from different spots in a single, segmented SnO_2 nanowire, fabricated as described previously,[23] and placed on a Pyrex slide. Spectra were excited with 514.5 nm argon ion laser light focused by a 100× (0.8 NA) lens and recorded on a Dilor LabRam micro-Raman spectrometer. The polarization vector was rotated using a half-wave plate positioned such that both the incident and backscattered light passed through the plate. Hence, the electric vector of the parallel component of the scattered light (denoted as ∥) was coincident in direction with that of the incident light. This component as well as the component perpendicular to it (denoted as ⊥) were selected out of the scattered signal with an analyzing polarizer situated between the half-wave plate and the spectrometer. To simplify the measurements and the transformation from laboratory to crystal-fixed coordinates, the origin of the lab-fixed coordinates was chosen such that the long axis of the nanowire lay along one of the canonical lab-fixed coordinates. Figure 1 presents the Raman scattering geometry used in this experiment with the definitions of the various angles. Further details of the setup are given elsewhere.[12]

3. RESULTS AND DISCUSSIONS

3.1. General Considerations in Raman Polarization Analysis of a Rutile Structure. The D_{4h}^{14} symmetry rutile (tetragonal) SnO_2 contains two formula units per primitive cell and lattice constants $a = b = 4.7373$ Å and $c = 3.1864$ Å.[24] Group theory predicts that the $\mathbf{k} = 0$ optical modes belong to the representations[18]

$$\Gamma = A_{1g} + A_{2g} + A_{2u} + B_{1g} + B_{2g} + 2B_{1u} + E_g + 3E_u$$

A_{1g}, E_g, B_{1g}, and B_{2g} modes are Raman active; A_{2u} and $3E_u$ modes are IR active; and $2B_{1u}$ and A_{2g} modes are inactive.

The Raman tensors, $\vec{R}$, of the pertinent phonon symmetries in rutile SnO_2 are as follows

$$\vec{R}(A_{1g}) = \begin{bmatrix} a & & \\ & a & \\ & & b \end{bmatrix} \quad \vec{R}_1(E_g) = \begin{bmatrix} & & d \\ & & \\ d & & \end{bmatrix} \quad \vec{R}_2(E_g) = \begin{bmatrix} & & \\ & & d \\ & d & \end{bmatrix}$$

$$\vec{R}_1(B_{2g}) = \begin{bmatrix} & e & \\ e & & \\ & & \end{bmatrix} \quad \vec{R}_2(B_{1g}) = \begin{bmatrix} c & & \\ & -c & \\ & & \end{bmatrix}$$

The observed Raman intensity for the jth phonon is proportional to

$$I_j \propto |\hat{e}_S \vec{R}_j(\omega_L)\hat{e}_l|^2 \quad (1)$$

where $\hat{e}_{l,s}$ are unit vectors in the incident (l) and scattered (s) direction, respectively. For the backscattering configuration, with the long axis of the nanostructure lying along the X direction, as is presented in Figure 1, we solve eq 1 for the two configurations, parallel ($\psi_S = \psi_L$) and perpendicular ($\psi_S = \psi_L + 90°$), and calculate the Raman intensities of the various phonon bands.

We show below that crystalline isomorphism is not a sufficient condition for determining the anticipated band intensities which are strongly affected by the relative magnitudes of the Raman tensor components that, in turn, reflect material-dependent differences in electron−phonon interactions. To illustrate, we compare (Figure 2) the calculated dependence of the ∥ and ⊥ band intensities of the E_g, B_{2g}, and A_{1g} phonons as a function of polarization angle for light incident normal to the (110), (100), (001), and (101) planes of SnO_2, RuO_2, and TiO_2. Literature values for the susceptibility tensor components[25] (normalized to $a = 1$ (a is the $\chi_{xx(yy)}$ of the A_{1g} phonon)) are listed in Table 1. The corresponding Eulerian angles and the incident and scattered polarization vectors assumed in the calculation are listed in Table 2 (with c/a :the ratio of the two lattice constants).

Figure 2 summarizes pictorially the strategy one would normally use to determine the growth direction from the polarization angle dependence of the A_{1g}, E_g, and B_{2g} phonon bands of rutile-like structures. The A_{1g} phonon is found in all ∥ spectra and is expected to have a low (or zero) intensity in the ⊥ spectra. However, it is predicted to be sensitive to polarization angle only for growth in the (100), (110), and (101) planes. Because for the (001) direction the polarization rotates in the ab (xy) plane and the susceptibility tensor elements χ_{xx} and χ_{yy} are degenerate, the signal is independent of ψ_L. In contrast, the χ_{zz} tensor element contributes when growth occurs along the (100) and (110) planes. Moreover, the greater the difference between

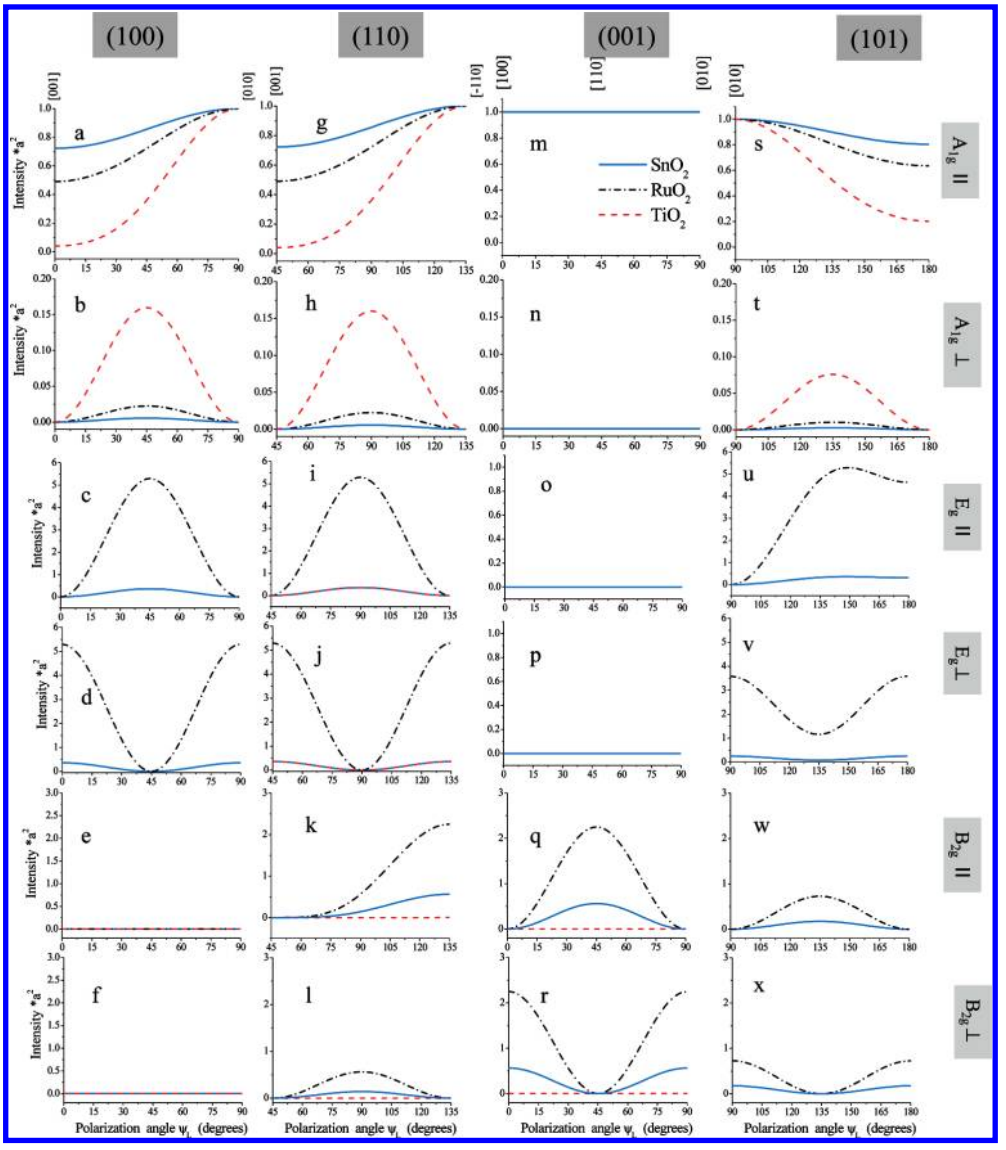

Figure 2. ψ_L dependence of the intensities of the E_g, B_{2g}, and A_{1g} phonons (in units of $a^2 = \chi^2_{xx(yy)}$ of the A_{1g} phonon), for parallel (∥) and perpendicular (⊥) spectra, computed for the most common (100) (a−f), (110) (g−l), (001) (m−r), and (101) (s−x) surfaces for TiO_2, SnO_2, and RuO_2. The intensity scales for A_{1g}∥, A_{1g}⊥, E_g (∥, ⊥), B_{2g} (∥, ⊥) are in the ratios 1.0:0.2:6.0:3.0. Representative growth directions within the planes are also shown.

Table 1. Literature Values of the Relative Susceptibility Tensor Components for SnO_2, RuO_2, and TiO_2,[25] Normalized to $a = 1$ (a is the $\chi_{xx(yy)}$ of the A_{1g} Phonon)[a]

tensor component	SnO_2	RuO_2	TiO_2
a	1	1	1
b	0.85	0.7	∼0.2
d	0.6	2.3	0.6
e	0.75	1.5	∼0.02
c/a	0.672	0.691	0.644

[a] The ratio of the two lattice constants c/a is also shown.

this component and the $\chi_{xx(yy)}$ components, the more useful this phonon is in determining growth direction. It is the relative magnitude of these two components that accounts for the differences in intensity change as a function of ψ_L among the three materials listed in Figure 2. Hence, for TiO_2, for which the ratio of the two components is great, the polarization angle dependence of the A_{1g} is large, and this band alone can be used to determine the nanowire's growth direction. This would be less so for SnO_2. For absorbing crystals (in some cases due to sub-bandgap transitions, which are ascribed to defects, see section 3.3), the susceptibility tensor elements of this phonon would be complex-valued. This complicates the analysis somewhat but does not weaken the overall validity of the approach.

The E_g phonon tensor possesses only $\chi_{xz(zx)}$ and $\chi_{yz(zy)}$ components and should, therefore, be silent in the (001) spectra and most intense for (100) with the polarization rotating in the bc (yz) plane. This is the most indicative band for RuO_2.[17,21] The B_{2g} tensor possesses only $\chi_{xy(yx)}$ components. It should, therefore, be absent for (100) and strongest for (001).

Table 2. Eulerian Angles Incident and Scattered Polarization Vectors for Various Dominant Growth Planes of the Rutile Structures

growth plane	(100)	(110)	(111)	($k0m$)	(001)
θ	90°	90°	90° $-\arctan[c/(\sqrt{2}\,a)]$	90° $-\arctan[(kc)/(ma)]$	0°
α	180°	135°	135°	180°	0°
ϕ	0°	45°	45°	0°	0°
$\hat{e}_{l,s}$	$\begin{pmatrix} 0 \\ -\sin(\psi_{L,S}) \\ \cos(\psi_{L,S}) \end{pmatrix}$	$\begin{pmatrix} \frac{-\sqrt{2}}{2}\cos(\psi_{L,S}+45) \\ \frac{\sqrt{2}}{2}\cos(\psi_{L,S}+45) \\ \sin(\psi_{L,S}+45) \end{pmatrix}$	$\begin{pmatrix} \frac{-\sqrt{2}}{2}\cdot[\cos(\theta)\cdot\sin(\psi_{L,S}+45)+\cos(\psi_{L,S}+45)] \\ \frac{\sqrt{2}}{2}\cdot[-\cos(\theta)\cdot\sin(\psi_{L,S}+45)+\cos(\psi_{L,S}+45)] \\ \sin(\theta)\cdot\sin(\psi_{L,S}+45) \end{pmatrix}$	$\begin{pmatrix} -\cos(\theta)\cdot\cos(\psi_{L,S}) \\ -\sin(\psi_{L,S}) \\ \sin(\theta)\cdot\cos(\psi_{L,S}) \end{pmatrix}$	$\begin{pmatrix} \cos(\psi_{L,S}) \\ \sin(\psi_{L,S}) \\ 0 \end{pmatrix}$

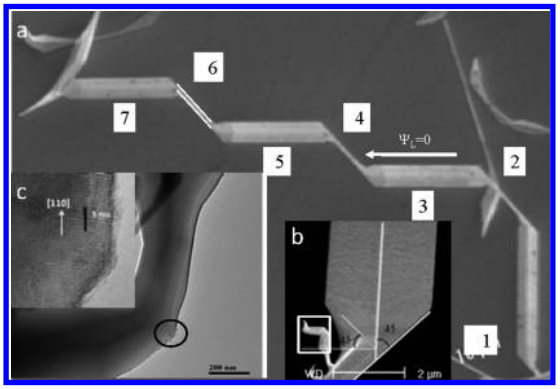

Figure 3. (a) SEM image of a (seven-sectioned) segmented SnO_2 wire residing on a Pyrex slide. (b) A higher magnification of a junction between a thick and a thin segment. In the white square is a small protrusion of a small segmented wire that also shows a 45° twist. From a similar wire, an HRTEM image was taken and shown in (c). The measured interplanar distance suggests that the growth direction is [110].

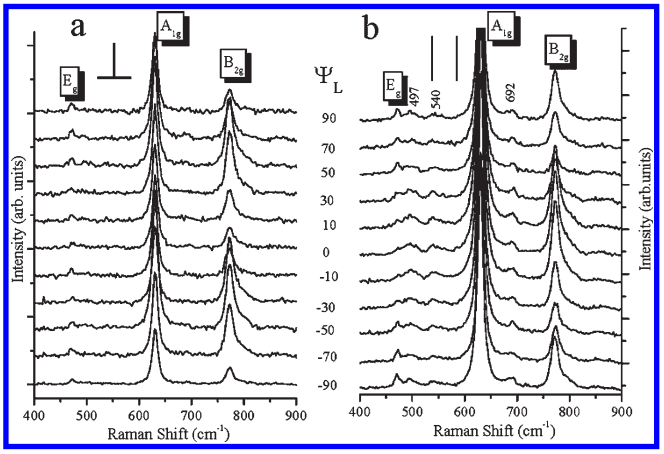

Figure 4. Polarized Raman spectra from the segment #3 in the ⊥ (a) and ∥ (b) polarization configurations.

Summarizing, the data presented in Figure 2 imply that for TiO_2 the A_{1g} band is a good growth-direction determining band; however, for RuO_2 the E_g band plays that role, and when it is absent (e.g., for the (001) plane), the B_{2g} suffices. For SnO_2 the B_{2g} is clearly the only good option. Further exploration of this approach for other rutile structures is straightforward, assuming the relative magnitudes of the Raman susceptibility components are known.

3.2. Structural and Polarized Raman Analysis of a Single Segmented Wire. Figure 3a shows a SEM image of a (seven-sectioned) segmented SnO_2 wire[23] residing on a Pyrex slide. The segments, which are each disposed at 45° relative to its neighbor, are coplanar. Thus, all of the thick segments are either parallel or make a 90° angle to one another.

The observed coplanarity and relative disposition of the thick sections can only be satisfied if the growth direction belongs either to the ⟨110⟩ or the ⟨100⟩ family within the (001) plane. Only one other growth direction from the ⟨302⟩ family can result in turning angles between adjacent thick and thin segments close to 45°. In that case, however, growth is not expected to result in a planar structure if one (credibly) assumes equal probability of encountering growth in the [302] and the [032] directions. We therefore conclude that it is highly unlikely that the growth was in the ⟨302⟩ direction.

A higher magnification of a junction between a thick and a thin segment is shown in Figure 3b. The 45° bend between them is coincident with a twist of the prismatic structure in a way that enables one to roughly deduce the base angle of the wire, which is found to be ∼45°. In the white square, we show a small protrusion of a small segmented wire that also shows a 45° twist. From a similar wire, an HRTEM image was taken and shown in Figure 3c.[26] The measured 0.335 nm interplanar distance matches the [110] growth direction (as previously proposed on the basis of incomplete analysis in ref 23).

Figure 4 shows the ∥ and ⊥ polarized Raman spectra of segment #3. Spectra were also recorded from segment #1, which are consistent with those obtained from #3, but the polarization angle dependence is shifted by 90° from the former. Raman measurements on segment #2 did not produce good enough quality spectra to enable a comprehensive discussion.

The segmented wires are evidently rutile, with the bands at 470, 629, and 771 cm^{-1} assignable, respectively, to first order E_g, A_{1g}, and B_{2g} phonons. The B_{1g} mode which is expected at 123 cm^{-1} [27] is not observed due to its low cross section (typical $I_{B1g}/I_{A1g} \approx 10^{-3}$ [18]). Besides these three intense peaks, three weak atypical Raman lines are observed at 497, 540, and 692 cm^{-1}, which were previously reported.[28] The 497 and 692 cm^{-1} bands are assigned in some studies to the IR active A_{2u} transverse optical (TO) and longitudinal optical (LO) phonons and the 540 cm^{-1} band to the inactive B_{1u} mode. The presence of IR modes and other forbidden Raman modes had been attributed to the relaxation of the Raman selection rules purportedly due to the reduced dimension of the nanostructure, as well as to lattice disorder and to a high concentration of defects such as oxygen vacancies.[29]

On the basis of the HRTEM results plus the above structural arguments, the polarization angle dependence of the

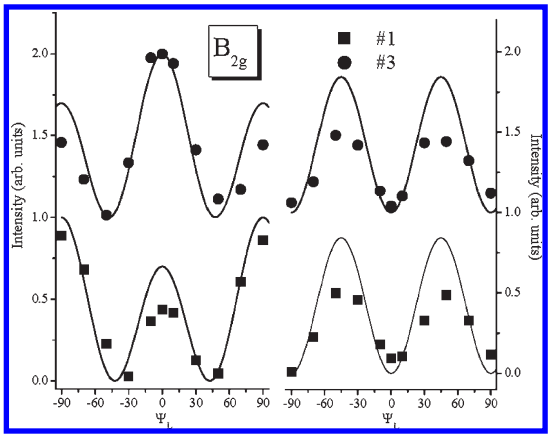

Figure 5. Correlation between the B_{2g} intensity with the calculated profiles (solid lines) for segments #1 and #3.

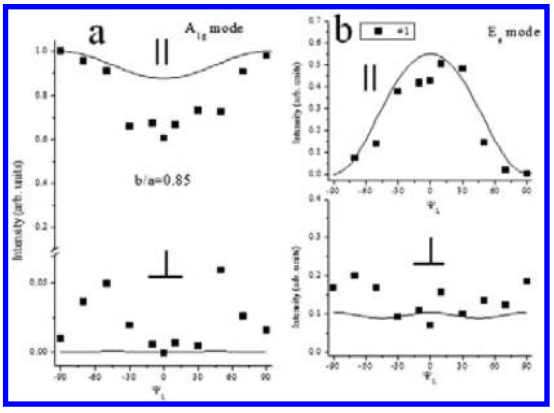

Figure 6. Correlation between the A_{1g} (a) and the normalized E_g (b) modes intensity with the calculated profiles (solid lines) for segment #1.

various Raman bands should correspond to those shown in Figure 2m−r, with angle ψ_L rotated by 45°; i.e., $\psi_L = 0°$ in the measurement corresponds to $\psi_L = 45°$ in Figure 2. Accordingly, one expects the intensity of the A_{1g}‖ band to be independent of ψ_L and the E_g mode to be undetectable. Furthermore, the B_{2g} band, which, as discussed above, is the most discriminating band, should have similar intensities at $\psi_L = 0°$ and $\psi_L = 90°$. However, the ψ_L dependence of the intensity of the B_{2g} mode for segments #1 (#3)[30] shows (Figure 5) that its intensity at $\psi_L = 0°$ (90°) is ∼50% lower than its value at $\psi_L = 90°$ (0°), which is not in line with what is expected for a structure growing along the [110] direction and interrogated with light incident perpendicular to the (001) plane. According to expectation, the perpendicular growth direction to the [110] direction in the (001) plane is [$\bar{1}$10], which is degenerate unless the degeneracy is removed for some reason. Figure 6 presents the ψ_L intensity dependence for the A_{1g} (Figure 6a) and E_g (Figure 6b) modes, for segment #1. Here again the results differ from what is expected (Figure 2m−r).

It is clear that other effects are at play here causing the experimental results for the B_{2g} (Figure 5) to deviate from what is calculated (Figure 2). These additional effects will be addressed below primarily to account for the observations for the B_{2g} band but also applied to the (less compelling) polarization dependence of the A_{1g} and E_g bands (Figure 6).

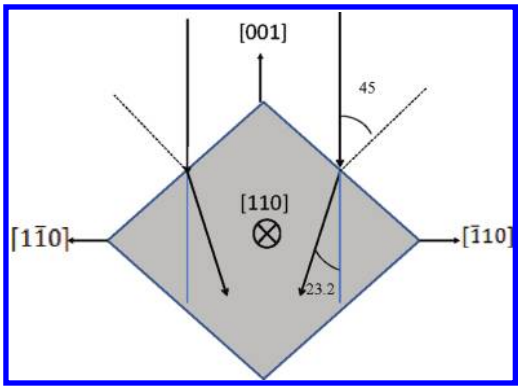

Figure 7. Schematic illustrating the incidence of the excitation laser beam on the thick segment of the SnO_2 wire in a backscattered configuration. The incident light impinges the surface at 45° and propagates at an angle of 23.2° with respect to the excitation beam direction.

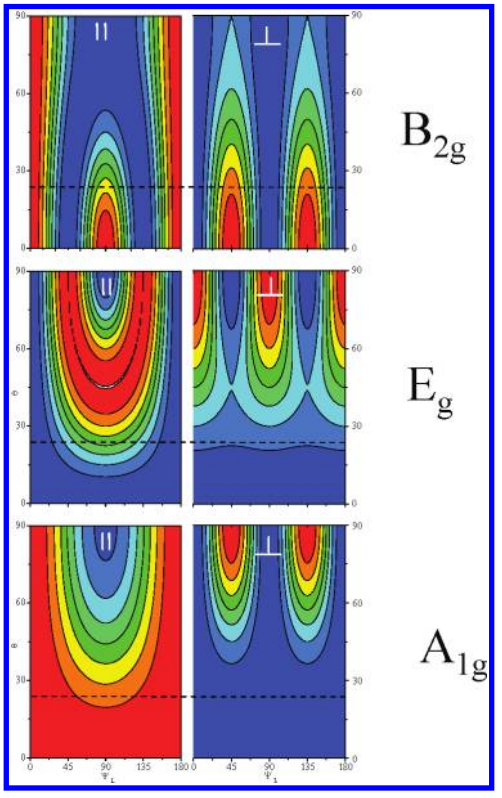

Figure 8. Dependence of the intensity of the B_{2g}, E_g, and A_{1g} phonons as a function of ψ_L when the [001] is tilted at an angle θ around the [110] direction. Red represents maximal and blue represents minimal intensities. The Raman cross sections at $\theta = 23.2°$ are shown as dashed lines corresponding to the parameters pertinent to segment #3.

As pointed out above, the base angle of the SnO_2 prismatic structure is 45°. This plus the large refractive index of SnO_2 (n = 1.90[31] for λ = 514.5 nm) will strongly affect the polarization angle dependence of the various phonon band intensities since refraction will reduce the angle of incidence inside the wire. Using the above value for the refractive index, one calculates (Snell's law[32]) that when a laser beam impinges the crystal's surface at 45° from the surface normal the internal angle will be reduced to 21.8°

dx.doi.org/10.1021/jp202310t |J. Phys. Chem. C 2011, 115, 17270–17277

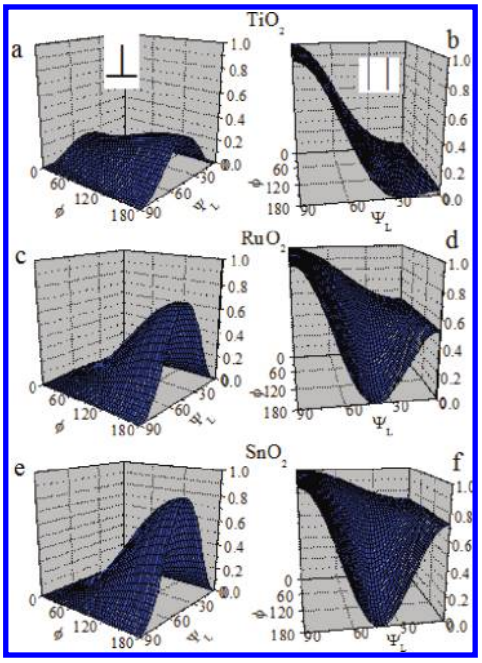

Figure 9. Effect of varying the relative phase φ on the expected Raman intensity in the ∥ and ⊥ spectra for the (100) plane of TiO_2 (a,b), RuO_2 (c,d), and SnO_2 (e,f) for b/a ratios equal 0.2, 0.70, and 0.85 (see Table 1).

with respect to the surface normal and 23.2° with respect to the excitation beam direction (Figure 7).

The effect of refraction which shifts the incident direction by 23.2° from the laboratory-fixed Z-axis around the [110] axis can be mimicked by tilting the [001] axis with respect to the Z-axis through an equivalent angle. The result is illustrated in Figure 8 for the B_{2g}, E_g, and A_{1g} phonons. The Raman cross sections at θ = 23.2° are shown as dashed lines in the figure. For the ∥ polarization, the X ([110]) and Y ([$\bar{1}$10]) degeneracy of the B_{2g} phonon is removed, causing the intensity at ψ_L = 90° to decrease relative to that at ψ_L = 0°. For ⊥ the Raman intensity is decreased but expected to be of equivalent magnitude for ψ_L = 90° and ψ_L = 0°.

The E_g phonon, which should be completely absent, is made slightly active due to the fact that after tilting the $xz(yz)$ components no longer strictly correspond to their subscripted coordinates. Weak signals due to this band are now found in the spectra for both polarizations. Finally, for ∥ polarization, the A_{1g} mode, which should have no ψ_L dependence, decreases in intensity since $\chi^2_{zz} < \chi^2_{xx(yy)}$. In the ⊥ spectrum the intensity (which is very low but not null for θ = 0°) is expected to increase with θ.

The quantity $I_{B_{2g}}$(23.2°), which is presented as a dashed line in Figure 8, as a function of ψ_L (solid lines) fits the observed data (points) satisfactorily (Figure 5). This is so despite the fact that there is an additional effect that is also expected to contribute to the quantitative evaluation of the scattering signals. The reflectance at the sample's interface of both the incident and Raman-scattered light depends strongly on the relative p- and s-polarization components comprising those beams, which, in turn, will impact ψ_L and ψ_S.[32] While the treatment with a single paraxial trajectory provides results adequate for the determination of the growth direction, for a full and precise quantitative determination of the polarization angle dependence of the Raman intensities

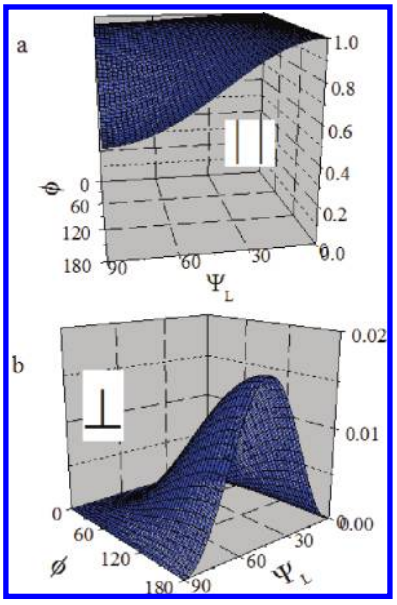

Figure 10. Effect of φ on the signals of the ∥ (a) and ⊥ (b) SnO_2 with the [001] axis tilted by 23.2° (relevant for the configuration of segment #3).

one needs to take into account the Gaussian profile of the beam incident at a dielectric interface, together with the effect of internal reflection inside the dielectric medium. Since the above analysis is also sensitive to the shape of the wire, a knowledge of the physical cross section of the wire is necessary. This problem will be tackled in a separate paper.

The results of an equivalent analysis for the E_g and A_{1g} phonons is shown in Figure 6 for segment #1 (90° tilted with respect to segment #3). The calculated profile of the ψ_L dependences is in good agreement with experiment. The only inconsistency is the higher intensity measured from the ⊥ configuration of the A_{1g} mode, an observation that is discussed next.

3.3. Effect of a Complex Valued Raman Tensor for the A_{1g} Mode. In a previous study on GaN nanowires (band gap = 3.4 eV), we showed that the polarization-dependent Raman intensities of the A_1 mode excited with 2.41 eV laser light could only be understood if a complex valued Raman tensor was assumed.[12] That most nanowires contain a high concentration of defects has been widely reported. For example, a yellow luminescence (YL) band was reported in the photoluminescence (PL) spectrum of GaN nanowires that is fully consistent with the complex-valued dielectric function we reported in ref 12. This finding and interpretation has been recently reproduced for a bundle of GaN nanowires.[33]

SnO_2 is another wide band gap (3.6 eV) material with strong sub-bandgap transitions accessible with 2.41 eV laser excitation. Sub-bandgap PL was reported for nanostructured and powdered SnO_2. For example, emissions observed from SnO_2 microrods[34] in the 520−630 nm range were ascribed to defects and oxygen vacancies in the near-surface region. Oxygen vacancies, located primarily at the surface, were proposed to interact with interfacial tin vacancies leading to the formation of trapped midgap states, responsible for yellow−green emission at room temperature.[28] In a like vein cathodoluminescence spectra obtained from nanostructured SnO_2 were explained in terms of oxygen vacancies. Several bands centered between 1.90 and 2.75 eV were ascribed to recombinations between conduction band and bulk shallow levels to levels near the top of the valence band.

Assuming a complex-valued Raman tensor, the A_{1g} bands are expected to be sensitive to the phase as well as the relative magnitudes of the tensor elements (this effect is not relevant to the B_{2g} and E_g bands[12]).

Writing the two tensor elements as $|a|e^{i\varphi_a}$ and $|b|e^{i\varphi_b}$, the effect of the phase ,φ, on the Raman intensities can be computed.[12] Here we report in Figure 9a−f for ∥ and ⊥ spectra of the (100) plane computed with b/a = 0.85, 0.7, and 0.2, which correspond to SnO_2, RuO_2, and TiO_2. Clearly, the weakest effect is observed when $\chi_{xx(yy)}$ and χ_{zz} differ most greatly, e.g., for TiO_2 which has practically no φ dependence in the ∥ spectra. The latter shows significant intensity increases as a function of φ, in its ⊥ spectra.[35]

Figure 10 shows the effect of φ on the respective signals SnO_2 with the (001) axis tilted by 23.2°. Here, there is a clear effect of φ, which would not be present in the absence of a tilt (Figure 2m, n). Indeed, we observe in Figure 6a that the calculated intensity for the A_{1g} mode with ∥ polarization is lower than the experimental one, which may be attributed to the effect of φ, as shown in Figure 10. However, due to the fact that the strong dependence of reflectivity on ψ_L and ψ_S may lead to an effect in the same direction as φ, it is difficult to extract a precise value of the phase from this analysis in the ∥ configuration. Nevertheless, the ⊥ results unequivocally demonstrate the effect of phase.

4. CONCLUSIONS

We describe the use of polarized Raman spectroscopy as a simple means for determining the growth direction in nanowires with the rutile structure. We show that the polarization angle dependence of various phonon bands can vary greatly even for isomorphic structures such as SnO_2, TiO_2, and RuO_2. As a result, different phonon modes function as the most structure-indicative modes for these three systems, as determined from the polarization angle dependence of their intensities.

Polarized Raman measurements were carried out on a single tetragonal (rutile) SnO_2 segmented nanowire with the prismatic microscale segments grown along the [110] direction in the (001) plane. We demonstrate the manifestation in the Raman polarization map of the removal of the degeneracy between [110] and the perpendicular [$\bar{1}$10] directions, which stems from the refraction of the incident beam inside the wire. The latter effect comes into play when the wire's effective diameter is significantly larger than the wavelength of the exciting light.

AUTHOR INFORMATION

Corresponding Author
*E-mail: t.livneh@nrcn.org.il.

ACKNOWLEDGMENT

This work was supported by the Institute for Collaborative Biotechnologies through grant DAAD19-03-D- 0004 from the U.S. Army Research Office and made extensive use of the MRL Central Facilities at UCSB supported by the National Science Foundation under award no. DMR-0080034 and DMR-0216466 for the SEM microscopy.

REFERENCES

(1) Pan, Z. W.; Dai, Z. R.; Wang, Z. L. *Science* **2001**, *291*, 1947.
(2) Dai, Z. R.; Gole, J. L.; Stout, J. D.; Wang, Z. L. *J. Phys. Chem. B* **2002**, *106*, 1274.
(3) Wang, Z. L.; Pan, Z. W. *Adv. Mater.* **2002**, *14*, 1029.
(4) Dai, Z. R.; Pan, Z. W.; Wang, Z. L. *J. Am. Chem. Soc.* **2002**, *124*, 8673.
(5) Wang, Z. L. *Adv. Mater.* **2003**, *15*, 432.
(6) Cheng, B.; Russell, J. M.; Shi, W.; Zhang, L.; Samulski, E T. *J. Am. Chem. Soc.* **2004**, *126*, 5972.
(7) Kolmakov, A.; Moskovits, M. *Ann. Rev. Mater. Res.* **2004**, *34*, 151.
(8) Wang, Z. L.; Gao, R. P.; Pan, Z. W.; Dai, Z. R. *Adv. Eng. Mater.* **2001**, *3*, 657.
(9) Liu, Y.; Dong, J.; Liu, M. *Adv. Mater.* **2004**, *16*, 353.
(10) Kolmakov, A.; Potluri, S.; Barinov, A.; Mentes, T. O; Gregoratti, L.; Nino, M. A; Locatelli, A.; Kiskinova, M. *ACS Nano* **2008**, *2* (10), 1993–2000.
(11) Katsiev, K.; Kolmakov, A.; Fang, M. H.; Diebold, U. *Surf. Sci.* **2008**, *602* (14), L112–L114.
(12) Livneh, T.; Zhang, J. P.; Cheng, G. S.; Moskovits, M. *Phys. Rev. B* **2006**, *74*, 035320.
(13) Chou, J. Y.; Lensch-Falk, J. L.; Hemesath, E. R.; Lauhon, L. J. *J. Appl. Phys.* **2009**, *105*, 034310.
(14) Zardo, I.; Conesa-Boj, S.; Peiro, F.; Morante, J. R.; Arbiol, J.; Uccelli, E.; Abstreiter, G.; Fontcuberta i Morral, A. *Phys. Rev. B* **2009**, *80*, 245324.
(15) Fan, H. M.; Fan, X. F.; Ni, Z. H.; Shen, Z. X.; Feng, Y. P.; Zou, B. S. *J. Phys. Chem. C* **2008**, *112*, 1865.
(16) Wu, J.; Zhang, D. M.; Lu, Q. J.; Gutierrez, H. R.; Eklund, P. C. *Phys. Rev. B* **2010**, *81*, 165415.
(17) Kim, M. H.; Baik, J. M.; Lee, S. J.; Shin, H.-Y.; Lee, J.; Yoon, S.; Stucky, G. D.; Moskovits, M.; Wodtke, A. M. *Appl. Phys. Lett.* **2010**, *96*, 213108.
(18) Katiyar, R. S.; Dawson, P.; Hargrave, M. M.; Wilkinson, G. *J. Phys. C: Solid State Phys* **1971**, *4*, 2421.
(19) Presser, V.; Schuster, B.-E.; Casu, M. B.; Heinemeyer, U.; Schreiber, F.; Nickelaand, K. G.; Chasse, T. *J. Raman Spectrosc.* **2009**, *40*, 2015.
(20) Huang, Y. S.; Lin, S. S.; Huang, C. R.; Lee, M. C.; Dann, T. E.; Chien, F. Z. *Solid State Commun.* **1989**, *70*, 517.
(21) Huang, Y. S.; Pollack, F. H. *Solid State Commun.* **1982**, *43*, 921.
(22) Yen, P. C.; Chen, R. S.; Huang, Y. S.; Chia, C. T.; Chen, R. H.; Tiong, K. K. *J. Phys.: Condens. Matter* **2003**, *15*, 1487.
(23) Lilach, Y.; Zhang, J. P.; Moskovits, M.; Kolmakov, A. *Nano Lett.* **2005**, *5* (10), 2019.
(24) Wyckoff, R.W.G. *Crystal structures*; Interscience: New York, 1965; Vol. 1, p 251.
(25) The components for RuO_2 were acquired by extracting the intensity ratio I_{B2g}/I_{A1g} of $a_{x'x'}$ from the (110) single crystal surface and the I_{Eg}/I_{A1g} of $a_{x''x''}$ and I_{Eg}/I_{B2g} of $a_{x''y'}$ from the (101) single crystal surface.[21] Differences of relative intensities between different spectra should not affect the result. The components for TiO_2 were acquired from Figure 1 of ref 19 which presents a series of spectra measured as a function of polarization from a (110) surface. The components for SnO_2 were acquired by extracting the relevant intensity ratios from ref 18 while assuming that all spectra were shown with similar sensitivity in the presented figures.
(26) Due to the difficulty of measuring the HRTEM from the thick segments, a protrusion of small wire had been analyzed. We note that occasionally, planarity may not be preserved during the wire's twists and turns.
(27) Peercy, P. S.; Morosin, B. *Phys. Rev. B* **1973**, *7*, 2779.
(28) Wang, F.; Zhou, X.; Zhou, J.; Sham, T. K.; Ding, Z. *J. Phys. Chem. C* **2007**, *111*, 18839.
(29) Hu, J. Q; Ma, X. L; Shang, N G; Xie, Z. Y.; Wong, N .B; Lee, C. S.; Lee, S .T *J. Phys. Chem. B* **2002**, *106*, 3823.
(30) The best fit was determined for both ∥ and ⊥ configurations after subtracting a background that probably arises from polarization leakage.
(31) Jiménez, V. M.; Espinos, J. P.; Caballero, A.; Contreras, L.; Fernandez, A.; Justo, A.; Gonzalez-Elipe, A. R. *Thin Solid Films* **1999**, *353*, 113.
(32) Hecht, E. *Optics*; Addison Wesley: Reading, MA, 1987; p 100.

(33) Tite, T.; Lee, C. J.; Chang, Y.-M. *J. Appl. Phys.* **2010**, *108*, 033504.
(34) Duan, J.; Huang, H.; Gong, J; Zhao, X.; Cheng, G.; Yang, S *J. Phys. D: Appl. Phys.* **2007**, *40*, 3998.
(35) We note that for $\psi_L = 0, 90$ the result for the (100) plane is independent of φ (see Figure 9). Hence, φ can be determined from a complete polarization map without a priori knowledge of the magnitudes of the *a* and *b* components (see Table 1).